JAERI-M
82-147

THERMAL INSTABILITY ANALYSIS IN A D-T TOKAMAK REACTOR WITH DENSITY DYNAMICS

November 1982

Akiyoshi HATAYAMA*, Masayoshi SUGIHARA
and Toshio HIRAYAMA

日本原子力研究所
Japan Atomic Energy Research Institute

JAERI-Mレポートは，日本原子力研究所が不定期に公刊している研究報告書です。
入手の問合わせは，日本原子力研究所技術情報部情報資料課（〒319-11茨城県那珂郡東海村）あて，お申しこしください。なお，このほかに財団法人原子力弘済会資料センター（〒319-11 茨城県那珂郡東海村日本原子力研究所内）で複写による実費頒布をおこなっております。

JAERI-M reports are issued irregularly.
Inquiries about availability of the reports should be addressed to Information Section Division of Technical Information, Japan Atomic Energy Research Institute, Tokai-mura, Naka-gun Ibaraki-ken 319-11, Japan.

編集兼発行　日本原子力研究所
印　　刷　(株)原子力資料サービス

JAERI-M 82-147

Thermal Instability Analysis in a D-T Tokamak Reactor with Density Dynamics

Akiyoshi HATAYAMA*, Masayoshi SUGIHARA
and Toshio HIRAYAMA

Division of Large Tokamak Development,
Tokai Research Establishment, JAERI

(Received September 29, 1982)

Basic models and formulations, which take account of the effects of the density dynamics (e.g. density perturbation, particle recycling, convective energy loss, etc.) are developed for the thermal instability analysis in a D-T tokamak reactor. The one-dimensional transport equations of ion density, electron and ion temperatures are linearized with respect to the perturbations and an eigenvalue analysis is used to calculate the growth rate of the instability. Critical curve of the stable and unstable regions on the density-temperature plane is determined for the case of the INTOR scaling law. It is also shown that the density mode of the trapped-ion scaling case is completely stabilized by the effect of particle recycling. They are reexamined by the time dependent transport code. These results show that the formulations developed are well effective to investigate the effects of the density dynamics on the thermal instability.

Keywords; Thermal Instability, D-T Tokamak Reactor, Density Dynamics, Density Perturbation, Particle Recycling, One Dimensional Transport Equations, Eigen Value Analysis, Critical Curve, Stable Region, Unstable Region, INTOR Scaling Law, Trapped-ion Mode Scaling Law, Time Dependent Transport Code

---

* Toshiba Corp.

密度ダイナミックスを考慮に入れたD－Tトカマク炉の熱的不安定解析

日本原子力研究所 東海研究所 大型トカマク開発部
畑山明聖*・杉原正芳・平山俊雄

（１９８２年９月２９日受理）

トカマク型核融合炉における熱的不安定性に関して，密度摂動，粒子リサイクリング，対流エネルギー損失等，密度のダイナミックスの効果を考慮に入れることのできる解析手法を開発した。不安定性の成長率は，イオン密度及び電子・イオン温度に対する１次元輸送方程式を摂動について線形化して得られる固有値方程式を解くことによって計算される。この手法を，イントールスケーリング則の場合に適用し，密度－温度平面上における熱的安定及び不安定領域を定めるとともに，その臨界曲線を求めた。また，捕捉イオン不安定則の場合，密度の摂動がある種の熱的不安定モードを励起することが知られている。ここでは，この種のモードが粒子リサイクリングを考慮するとき，安定化され得ることを示した。さらに，これらの結果を，１次元輸送コードにより摂動の時間変化を直接追跡するという方法を用いて，再検討した。以上から，ここで開発した手法が密度ダイナミックスの効果を正しく考えに入れた熱的不安定性の解析に対して十分有効な手法であることが示された。

＊東京芝浦電気（株）

Contents

目　　次

1. Introduction

Many works have been done so far on the thermal instability in a D-T fusion reactor[1)-18)]. Especially, in tokamak reactors, the growth time of the instability and the unstable region have been obtained[12,13)], since the energy confinement scaling law has been clarified to a certain degree. Several methods for controlling these instabilities are proposed[16-20)], while definitive methods are not established yet. In the tokamak reactor design, the operation point on the density-temperature plane must first be determined by taking account of many physics and engineering requirements and restrictions, such as toroidal beta value, total fusion power, neutron wall loading. Among the rest, the restriction by the thermal instability will be important factor. When we cannot avoid to set the operation point in the unstable region, it is of primary importance to investigate beforehand the growth time and the feature of the unstable mode in order to establish the reliable method for the control and measurement of the instability. To obtain the growth time, the unstable region and the feature of the unstable mode, we must investigate them on the basis of the precise scaling law and analytic model, which can reproduce realistic reactor conditions. As for the scaling law, it is widely accepted that INTOR scaling is standard[21)], while it is uncertain that this scaling law is applicable to future higher temperature and α-particle heated plasmas. Therefore, at present, it is important to establish the reliable analytic method for investigating the thermal instability.

As for the analytic model, zero-dimensional point model analyses were first done, and then one-dimensional analyses have been developed. However, emphases have been placed on the analysis of only the temperature perturbation, i.e., the density perturbations have been omitted and the density profile fixed or artificially created by pellet injection or neutral beam injection with complete pumping of the diffusing particles. In an actual tokamak reactor, however, it will be reasonable to consider that 5 ~ 10% of the diffusing particles are pumped out and the remaining particles are recycled to the main plasma to enhance the fuel burn-up fraction[22)]. This pumping ratio might also be reasonable due to the engineering restriction on the pumping capacity[23)]. Thus, for the more precise analytic model, it is necessary to develop the particle recycling model and take account of the density

dynamics such as the effects of the density profile, density variation, convective energy loss, particle recycling.

The purpose of this paper is to develop more refined one-dimensional model for the thermal instability analysis taking account of the density dynamics. The effects of the particle recycling are considered in the analysis by evaluating the diffusing particle flux at the plasma boundary and using the constraints of the total number density conservation. Linearizing the perturbed transport equations for ion density, electron and ion temperatures, we obtain the generalized eigen value equation, whose solution provides the growth rate and unstable region of the instability. We apply the formulations developed to the INTOR scaling law for the transport coefficients as a standard reference. Critical curve of the thermally stable and unstable region on the density and temperature plane for an INTOR-size reactor is obtained. We also determine a regime of stable operation, which satisfies the requirement of high Q (= fusion output power/input power) operation and the limitation of the toroidal β-value.
In addition, when the transport coefficients strongly depend on the density and temperature, the effect of the density dynamics on the instability will be far more important. In fact, it has been pointed out that a thermal instability driven by density perturbation can arise in the case of the trapped-ion mode scaling[9,24]. The effects of particle recycling are examined for this density-driven thermal instability. It will be shown that this mode is completely stabilized as the recycling rate approaches to unity. We reexamine our basic formulations and linear stability analysis by using time dependent one-dimensional transport code.

Formulations developed in this paper will serve to analyse the thermal instability more correctly when the more reliable energy and particle confinement scaling laws are obtained in future. These will provide useful information to establish the method for the measurement and control of the instability and also will be a useful tool for the physics design considerations.

2. Basic Equations and Models of Analysis

The basic equations are the one-dimensional particle and energy transport equations. These equations are given by

$$\frac{\partial n}{\partial t} = -\frac{1}{r}\frac{\partial}{\partial r} r\Gamma + S - S_f = F_1 + S \quad , \tag{2.1}$$

$$\frac{3}{2}\frac{\partial}{\partial t}(nkT_e) = \frac{1}{r}\frac{\partial}{\partial r} r\left[n\chi_e k \frac{\partial T_e}{\partial r} - \frac{5}{2} k\Gamma T_e \right] + \frac{\Gamma}{n}\frac{\partial}{\partial r}(nkT_e) - \frac{nk(T_e - T_i)}{\tau_{eq}} + P_{fe} + P^e_{ext} + P_J - P_{br} - P_{sy} = F_2 \quad , \tag{2.2}$$

$$\frac{3}{2}\frac{\partial}{\partial t}(nkT_i) = \frac{1}{r}\frac{\partial}{\partial r} r\left[n\chi_i k \frac{\partial T_i}{\partial r} - \frac{5}{2} k\Gamma T_i \right] + \frac{\Gamma}{n}\frac{\partial}{\partial r}(nkT_i) + \frac{nk(T_e - T_i)}{\tau_{eq}} + P_{fi} + P^i_{ext} = F_3 \quad , \tag{2.3}$$

where n is the plasma density and T_e and T_i are the electron and ion temperatures, respectively. Also, χ_e and χ_i are the electron and ion thermal diffusivities, τ_{eq} is the ion-electron energy relaxation time and k is the Boltzmann constant. The MKS units are used for all quantities except for T_e and T_i, which are given in eV. The remaining notations and their basic models used in Eqs.(2.1) - (2.3) are as follows;

(1) particle transport equation

For the density dynamics, we assume that the deuterium and tritium densities are equal every where ($n_D = n_T = n/2$) and consider the behavior of the total ion density ($n = n_D + n_T$). The ion particle flux Γ in Eq.(2.1) is expressed by

$$\Gamma = -D\frac{\partial n}{\partial r} + \Gamma^{in}_W \quad , \tag{2.4}$$

where D is the diffusion coefficient and Γ^{in}_W is the inward particle flux due to Ware pinch[25], which is given by

$$\Gamma^{in}_W = -C_W \frac{2.44\sqrt{\varepsilon}\, E_z}{(1 + 0.85\,\nu_e^*)B_p} \quad . \tag{2.5}$$

Here, ε is the inverse aspect ratio, E_z the toroidal electric field, B_p the poloidal magnetic field. Also, ν_e^* is the collisionality parameter of banana-plateau for the electrons and C_W is a numerical factor.

The particle fueling source S can be written as

$$S = S_n \cdot f(r) \quad , \tag{2.6}$$

where S_n is the total source amount in the plasma volume and f(r) is the source profile normalized by S_n ($f(r) = S/S_n$). Most of the previous works on the thermal instability assumed that S consists of only the external fueling source. However, in realistic tokamak operation, a large part of particles lost due to diffusion return to the plasma. We take into account such a recycling effect by using the constraint of the total number density conservation. That is, S_n can be determined by the equation,

$$\int S dV = R_c \int \frac{1}{r} \frac{\partial}{\partial r} r\Gamma dV + \int S_{ext} dV \quad , \tag{2.7}$$

where R_c is the recycling rate and S_{ext} represents the external fueling source. On the other hand, source profile f(r) in Eq.(2.6) is determined by neutral calculation code[26], which solves the neutral transport equation in cylindrical geometry.

The sink term S_f by D-T fusion reaction has the form,

$$S_f = \frac{1}{2} n^2 \langle \sigma v \rangle \quad . \tag{2.8}$$

The reaction rate $\langle \sigma v \rangle$ is approximated by the following equation[27],

$$\langle \sigma \rangle = \begin{cases} 0 & (T_i < 1.1 \text{ keV}) \\ 10^{-22} \times \exp(c_1 y^3 + c_2 y^2 + c_3 y + c_4) & (1.1 \text{ keV} \leq T_i < 150 \text{ keV}) \\ 6.268 \times 10^{-22} & (150 \text{ keV} \leq T_i) \end{cases} \tag{2.9}$$

where $y = \ell n(T_i/10^3)$, $C_1 = 0.038245$, $C_2 = -1.0074$, $C_3 = 6.3997$ and $C_4 = -9.750$.

(2) electron and ion energy transport equations

In Eqs.(2.2) and (2.3), P_{fe} and P_{fi} represent the α-particle

heating power densities for electrons and ions, respectively. We assume that the α-particle energy is delivered to the field particles instantaneously, since the finite slowing down time will not have large effects on the thermal instability[12]. The heat deposition profile of α-particles is assumed to be the same as their birth profile. Then, P_{fj} is given by

$$P_{fj} = \frac{1}{4} n^2 \langle \sigma v \rangle k E_\alpha \cdot R_j \quad , \quad (j = i,e) \quad , \tag{2.10}$$

where $E_\alpha = 3.52$ MeV and R_j is the fraction of the energy to the particles of j-th species. Using the assumption $n_D = n_T = n/2$, R_i and R_e can be given by

$$R_i = \frac{3\sqrt{\pi}}{2} \frac{m_e}{m_r} \left(\frac{v_{the}}{v_{th\alpha}}\right)^3 \left(\frac{v_{th\alpha}}{v_c}\right) h \quad , \qquad R_e = 1 - R_i \quad , \tag{2.11}$$

with

$$h = H(v,v_c) \Big|_{v = v_{\alpha i}}^{v = v_{th\alpha}} \quad , \tag{2.12}$$

$$H(v,v_c) = \frac{1}{6} \ell n \frac{v^3 + v_c^3}{(v + v_c)^3} + \frac{1}{\sqrt{3}} \arctan \left(\frac{2v - v_c}{\sqrt{3}\, v_c}\right) \quad , \tag{2.13}$$

where $v_{thj} = \sqrt{2kT_j/m_j}$, $v_{\alpha i} = \sqrt{2kT_i/m_\alpha}$, $v_c = (3\sqrt{\pi}\, v_{the}/4)^{1/3}$ (m_j is the particle mass of j-th particles and $m_r^{-1} = 1/m_D + 1/m_T$).

The external heating sources for electrons and ions are denoted by P^e_{ext} and P^i_{ext}. We assume only the ion heating and put $P^e_{ext} = 0$ in the present analysis. P^i_{ext} is assumed to be in the form as

$$P^i_{ext} = P_i(0) \cdot [1 - (r/a)^2]^4 \quad , \tag{2.14}$$

where $P_i(0)$ is the heating power density at $r = 0$ and a is the plasma minor radius. The peaked heating profile in the plasma center, which will correspond to the RF type external heating, is assumed in Eq.(2.14). Although the change of heating profile and heating species (electron or ion) will have a considerable effect on the thermal instability[13],

our primary concern is placed on the effect of density dynamics so that only one type of external heating given by Eq.(2.14) is employed here.

Another heating source term in Eq.(2.2) is Joule heating P_J. Using the plasma toroidal and poloidal current densities J_z and J_p, P_J is expressed by

$$P_J = \eta_z J_z^2 + \eta_p J_p^2 \quad , \tag{2.15}$$

where η_z and η_p are the plasma classical resistivities in the toroidal and poloidal directions.

The energy sink terms P_{br} and P_{sy} represent the bremsstrahlung radiation and the synchrotron radiation losses, respectively. Their expressions are

$$P_{br} = 1.42 \times 10^{-38}\ n^2 T_e^{1/2} \quad , \tag{2.16}$$

$$P_{sy} = 6.38 \times 10^{-16}\ B_T^{5/2} T_e^{2} \sqrt{\frac{n}{R}} \quad , \tag{2.17}$$

where B_T and R are the toroidal magnetic field and the major radius of the torus, respectively.

In the above basic equations and models, the effects of impurities are neglected to simplify the analysis. The scrape-off layer plasma is not included either, though it is easy to consider it. Furthermore, charge exchange, ionization and excitation losses of fuel particles are ignored for simplicity.

3. Linear Stability Analysis

The stability analysis of the equations (2.1) - (2.3) is carried out in the following manner. First, the density, temperatures and particle source are expanded about their steady state solutions,

$$n(r,t) = n_0(r) + \delta n(r,t) \quad , \tag{3.1a}$$

$$T_j(r,t) = T_{j0}(r) + \delta T_j(r,t) \quad , \quad (j = e,i) \tag{3.1b}$$

$$S(r,t) = S_0(r) + \delta S(r,t) \quad . \tag{3.1c}$$

These expressions are substituted into Eqs.(2.1) - (2.3) and the non-linear terms are neglected. The resultant linearized one-dimensional equations for δn and δT_j can be simply expressed by using a matrix form,

$$A\delta\dot{X} = B\delta X + \delta S \quad , \quad \delta X = \begin{pmatrix} \delta n \\ \delta T_e \\ \delta T_i \end{pmatrix} \quad , \quad \delta S = \begin{pmatrix} \delta S \\ 0 \\ 0 \end{pmatrix} \quad , \tag{3.2}$$

where dot denotes the time derivative $\partial/\partial t$ and

$$A = \begin{pmatrix} 1 & , & 0 & , & 0 \\ \frac{3}{2} kT_{e0} & , & \frac{3}{2} kn_0 & , & 0 \\ \frac{3}{2} kT_{i0} & , & 0 & , & \frac{3}{2} kn_0 \end{pmatrix} \quad , \quad B = \begin{pmatrix} \frac{\partial F_1}{\partial n} & , & \frac{\partial F_1}{\partial T_e} & , & \frac{\partial F_1}{\partial T_i} \\ \frac{\partial F_2}{\partial n} & , & \frac{\partial F_2}{\partial Te} & , & \frac{\partial F_2}{\partial Ti} \\ \frac{\partial F_3}{\partial n} & , & \frac{\partial F_3}{\partial Te} & , & \frac{\partial F_3}{\partial Ti} \end{pmatrix} . \tag{3.3}$$

Here, it should be noted that all the elements in A, B, δX and δS have radial dependence.

Next, we eliminate the perturbation of the particle source δS from Eq.(3.2). As was noted in section 2, the particle source term S consists of two parts —— the external one (gas puffing or pellet injection) and the recycling one. Although the source profiles of both particle sources will be a little affected by the density and temperature perturbations, we will ignore for simplicity the perturbations of both source profiles. It will be reasonable to assume that the total source amount by external one is not perturbed. Thus, the perturbation of particle source δS comes from the recycling one and is given as

$$\delta S = \delta S_{rcy} \cdot f(r) \quad , \tag{3.4}$$

$$\delta S_{rcy} = -\delta R_c \int \frac{1}{r} \frac{\partial}{\partial r} r\Gamma \, dV \quad , \tag{3.5}$$

where we have used Eq.(2.7). The right hand side of Eq.(3.5) can be transformed into the surface integral of Γ. To obtain the growth rate of the instability, we will use the finite difference approximation for the space derivatives in Eq.(3.3). Since the spatial gradient at the plasma boundary may contain rather large error in the approximation, we rewrite the right hand side of Eq.(3.5) by using Eq.(2.1). Then, Eq.(3.5) is replaced by the following expression,

$$\delta S_{rcy} = \frac{-R_c}{1 - R_c} \int (\delta \dot{n} + \delta S_f) \, dV \quad . \tag{3.5}'$$

In actual reactors, R_c is always smaller than unity, since a certain fraction of diffusing particles is pumped out by the exhaust system for herium ash. Substituting Eqs.(3.4) and (3.5)' into Eq.(3.2), Eq.(3.2) can be reduced to the following generalized eigen value equation;

$$AM \, \delta \dot{X} = BM \, \delta X \quad , \tag{3.6}$$

with

$$AM = \begin{pmatrix} 1 - f(r) \dfrac{R_c}{1 - R_c} \displaystyle\int dV & , & 0 & , & 0 \\ \dfrac{3}{2} k T_{e0} & , & \dfrac{3}{2} k n_0 & , & 0 \\ \dfrac{3}{2} k T_{i0} & , & 0 & , & \dfrac{3}{2} k n_0 \end{pmatrix} \quad , \tag{3.7a}$$

$$BM = \begin{pmatrix} \dfrac{\partial F_1}{\partial n} - f(r) \dfrac{R_c}{1 - R_c} \displaystyle\int dV \dfrac{\partial S_f}{\partial n} & , & \dfrac{\partial F_1}{\partial T_e} & , & \dfrac{\partial F_1}{\partial T_i} - f(r) \dfrac{R_c}{1 - R_c} \displaystyle\int dV \dfrac{\partial S_f}{\partial T_i} \\ \dfrac{\partial F_2}{\partial n} & , & \dfrac{\partial F_2}{\partial T_e} & , & \dfrac{\partial F_2}{\partial T_i} \\ \dfrac{\partial F_3}{\partial n} & , & \dfrac{\partial F_3}{\partial T_e} & , & \dfrac{\partial F_3}{\partial T_i} \end{pmatrix} , \tag{3.7b}$$

where $\int dV$, $\int dV \, (\partial S_f / \partial n)$ and $\int dV \, (\partial S_f / \partial T_i)$ represent the integral

operators on $\delta\dot{X}$ and δX, respectively.

The growth rate and eigen function of the instability can be obtained by numerically solving Eq.(3.6). To this end, we devide the radial region considered (i.e. $0 \leq r \leq a$) into several zones with the width Δr_j (subscript j means the j-th radial zone). Finite difference and sum approximations are used for the space deviatives and integrals, in Eq.(3.6). The steady state quantities, such as $n_0(r)$, $T_{j0}(r)$ and $f(r)$ in AM and BM, are given at each mesh point. The boundary conditions imposed are $\partial\delta X/\partial r = 0$ at $r = 0$ and $\delta X = 0$ at $r = a$. Then, the matrixes AM and BM have $3\cdot(N-1) \times 3\cdot(N-1)$ elements, where N is the total number of the radial zones. That is, each matrix element in Eqs.(3.7a) and (3.7b) becomes $(N-1) \times (N-1)$ minor matrix. For example, $1 - f(r)R_c/(1-R_c)\int dV$ in Eq.(3.7a) becomes as

$$1 - f(r)\,\frac{R_c}{1-R_c}\int dV \longrightarrow \begin{pmatrix} 1+\alpha_2, & \alpha_3, & \cdots\cdots, & \alpha_N \\ \alpha_2, & 1+\alpha_3, & \cdots\cdots, & \alpha_N \\ \alpha_2, & \alpha_3, & \cdots\cdots, & \alpha_N \\ \vdots & \vdots & \ddots & \vdots \\ \alpha_2, & \alpha_3, & \cdots\cdots, & 1+\alpha_N \end{pmatrix}, \qquad (3.8)$$

where $\alpha_j = -f(r_j)\cdot R_c/(1-R_c)\cdot\pi(r_j\Delta r_{j-1} + r_j\Delta r_j)$ and the finite sum approximation (trapezoidal formula), $\int dV\, F(r) = 2\pi\int dr\, r\, F(r) \rightarrow 2\pi\sum_{j=1}^{N}[r_j F(r_j) + r_{j+1}F(r_{j+1})]\Delta r_j/2$, have been used ($r_j$,$F(r)$ are the radial coordinates at j-th mesh point and the arbitrary function, respectively). Finally, we replace the time derivative $\partial/\partial t$ by γ. The resultant eigen value equation for the eigen value γ and the eigen vector $\delta X^T = [\delta n(r_2), \text{----}, \delta n(r_N), \delta T_e(r_2), \text{----}, \delta T_e(r_N), \delta T_i(r_2), \text{----}, \delta T_i(r_N)]$ can be solved by standard numerical method.

With use of the growth rate obtained, growth time τ_s of the instability is defined by

$$\tau_s = \frac{1}{\mathrm{Re}\ \gamma_{max}}, \qquad (3.9)$$

where $\mathrm{Re}\gamma_{max}$ is the largest real part of all eigen values. Actually, in some cases, the growth rate γ can become complex, as will be shown later. In those cases, though the eigen functions are also complex,

only their real part is physically meaningful. For example, the time evolution of the ion density eigen mode is given as

$$\sqrt{(\delta n_r)^2 + (\delta n_i)^2} \cdot e^{\gamma_r t} \cdot \cos(\omega t + \phi) \quad . \tag{3.10}$$

Here, δn_r, δn_i, γ_r, ω and ϕ are the real and imaginary part of eigen vector and eigen value, and the phase of eigen vector, respectively. Various eigen functions given by arbitrary phase of $(\omega t+\phi)$ can emerge in our eigen mode analysis. We will check them by one-dimensional time dependent transport code for Eqs.(2.1) - (2.3).

In our thermal stability analysis, we have neglected the perturbations of the electromagnetic parameters, such as E_z, B_p, J_z and J_p, since the current diffusion time will be very long for the reactor grade temperature. As mentioned in section 2, the perturbations of P^j_{ext} have also been ignored.

We obtain the quasi-steady states of the density, temperatures and so on by the time dependent transport code, in which the ion temperature and ion density are controlled by the feedback method, which is similar to POPCON code[28]. For example, the ion temperature is controlled by the combination of the proportional and derivative control and $P_i(0)$ in Eq.(2.14) is given by

$$P_i(0) = \left[C_1(T_a - \bar{T}_i) + C_2 \frac{\Delta t/\tau}{1+\Delta t/\tau} \frac{\partial}{\partial t} \left(\frac{3}{2} \bar{n} k \bar{T}_i\right) \right] \quad , \tag{3.11}$$

where C_1, C_2, T_a, $\bar{T}_i$ and $\bar{n}$ are the gains, the desired and the average ion temperatures, and the average ion density, respectively. Also, Δt and τ are the time step of the transport code and the appropriate time constant. The quasi-steady states can be obtained after long simulation time (about 10 s).

The numerical calculations and their results will be shown in the next section.

4. Results of Calculations

Based on the formulations developed in the previous sections, we analyzed the following two cases, (1) INTOR scaling case and (2) Trapped-Ion Mode scaling case, and see that our formulations are well effective for the instability analysis with the density dynamics.

(1) INTOR scaling case

As the first example, we employ INTOR scaling[29] for the transport coefficients in Eqs.(2.1) - (2.3);

$$\text{Electron thermal diffusivity} : \chi_e = 5\times 10^{19}/n_e \cdot f(\kappa) \quad , \tag{4.1}$$

$$\text{Ion thermal diffusivity} : \chi_i = 3\chi_{neo} \cdot f(\kappa) \quad , \tag{4.2}$$

$$\text{Particle diffusion coefficient} : D = \chi_e/5 \quad , \tag{4.3}$$

where χ_{neo} is the neoclassical ion thermal diffusivity. Noncircular effect of plasma cross section is simply taken into account by a factor of $f(\kappa) = \sqrt{(1+\kappa^2)}/2\,/\,\kappa$ (κ: ellpticity of the plasma cross section), which is the volume-surface ratio of the plasma. We do not include the ripple enhanced thermal diffusion, for simplicity, in the present analysis.

The recycling rate R_c is set to 0.95, which will be the typical value of the reactor[29], and the fuels are fed by gas puffing. The energy of neutrals, which are recycled back and fed into the plasma, is assumed to be 5 eV. The numerical factor of the Ware flux in Eq.(2.5) is taken as $C_W = 1.0$.

The device parameters used in the calculations are listed in Table 1, which are proposed by the recent design study of Fusion Experimental Reactor (FER) in JAERI and are similar to those of INTOR.

Typical profiles of electron and ion temperatures and ion density in the steady state ($\bar{n} \sim 1.0\times 10^{20}\mathrm{m}^{-3}$, $\bar{T}_i \sim 10$ keV and $\bar{T}_e \sim 8$ keV) are shown in Fig.1. There is always only one unstable mode in the unstable equilibrium state, which is purely growing ($\mathrm{Im}\gamma = 0$) and global mode. The unstable eigen functions for the equilibrium state of Fig.1 are shown in Fig.2 for the electron and ion temperatures and in Fig.3 for the ion density. Figure 4 shows the equi-growth time lines of the instability on the $\bar{n} - \bar{T}_i$ plane. The dotted line $\tau_s = \infty$ is the critical curve of the thermally unstable and stable regions. We restrict our

analysis to the sub-ignited region in Fig.4. By the feedback control of Eq.(3.11), we can obtain the quasi-steady state even in the over-ignited region and can examine its thermal stability. However, $P_i(0)$ in the steady state becomes negative in this case, which correspond to the central cooling of the plasma. There seems to be no such cooling scenario at present, so that we do not consider such a case in the present analyses. To determine the operating point, it is convenient to draw equi-Q lines on the $\bar{n} - \bar{T}_i$ plane, where Q is defined by

$$Q = \frac{5 \int (P_{fe} + P_{fi})\, dV}{\int (P^e_{ext} + P^i_{ext} + P_J)\, dV} \quad . \tag{4.4}$$

This is shown in Fig.5. When these figures (Fig.4, 5) are supplemented by equi-beta lines, we can choose the stable or weakly unstable operating regime within the β-limitation, which realize the required Q-value. Two examples are shown in Fig.6. Hatched regions (a) and (b) satisfy the following operating conditions,

i) stable operation, $Q \geq 30$, $\beta \leq 4\%$,

ii) stable operation, $Q \geq 10$, $\beta \leq 3\%$,

respectively.

The effect of the density perturbation on the thermal instability is small in this scaling law. This is because the dependence of D and χ_e on the density and temperature is weak (e.g. D, $\chi_e \propto 1/n$). Quantitively, if we put $\delta n = 0$ in Eq.(3.6) and omit the density perturbation in the analysis, the growth rates become larger by 10% at most. This increase of the growth rate is mainly due to the fact that the dominant term in Eq.(2.1) is the fusion term S_f in this scaling law. The effect of the particle recycling is also small and the growth rate is little affected by the recycling rate.

(2) Density mode of the trapped ion scaling case

In the present sub-section, we analyse the density mode of trapped ion scaling as an example, and show that the density perturbation can be important when the density and temperature are strongly coupled in the transport coefficients. It has been pointed out that the equilibrium state of the trapped ion mode scaling is stable for the temperature perturbation, while is unstable for the density perturbation[9,24].

However, when we consider the particle recycling, this mode will be stabilized, since the particle recycling works as a feedback control to the density perturbation. This will be shown by our stability analysis. The plasma and device parameters used in the analysis are shown in Table 2. The fuel particles are fed by the pellet injection as well as the particle recycling. To obtain the equilibrium state, the particle density is kept constant by the feedback control. Figure 7 shows the growth rate of the instability as a function of the recycling rate R_c. The instability is stabilized when $R_c \gtrsim 0.95$. Figure 8 shows the typical unstable eigen functions of the ion density and ion temperature (only one mode is unstable) for $R_c = 0.0$. The unstable mode is strongly oscillatory ($\omega \sim \gamma$).

These results are reexamined by one-dimensional time dependent transport code. Unstable eigen mode perturbations shown in Fig.8 are added to the equilibrium state, and the feedback control of the density is turned off simultaneously. Time evolutions of the average ion density are shown in Fig.9. Time evolutions of the density perturbation are shown in Fig.10. To compare the results of Fig.10 with the eigen functions given by Eq.(3.10), we depict Eq.(3.10) for various phases with the growing term (exponential term) dropped. They are shown in Fig.11. From Figs.10 and 11, it is seen that the perturbations maintain the shape of the linear eigen function for rather long time. The growth rates obtained by the time dependent transport code, however, are smaller than those by eigen equation calculation by a factor of 1.5 to 2 as shown by circles in Fig.7. This is due to the nonlinear effects i.e., particle and energy diffusion, since the growth time and the diffusion time is comparable. The fundamental profiles of the background plasma density and temperature do not change so much, so that there is always only one unstable eigen mode. Other modes, which distort the shape of the unstable eigen mode, damp one after another, so that the shape of the linear unstable eigen function remains almost unchanged.

5. Summary

The model of particle recycling and the basic formulations for the one-dimensional thermal instability analysis in a tokamak reactor taking into account the density perturbation were developed. The growth rate and eigen functions of the instability were calculated by numerically solving the linearized eigen value equations of ion density, electron and ion temperatures. We applied the formulations to the following two cases of transport scaling law. The results obtained are summarized as follows.

(1) INTOR scaling law

Thermal stability properties were examined over wide range of the $\bar{n} - \bar{T}_i$ plane. Critical curve of the thermally unstable and stable regions on the $\bar{n} - \bar{T}_i$ plane were determined. We also determined an operating regime, which meets the following physics design requirements, (a) thermally stable operation, (b) attainment of required Q-value and (c) operation within the critical toroidal β-value.

In this scaling law, the effects of the density perturbation and the particle recycling are small. The growth rate of the instability decreases by only about 10% in comparison with the case of $\delta n = 0$.

(2) trapped-ion mode scaling law

If the density and temperature are strongly coupled in the transport coefficients, the effect of the density perturbation becomes significant. This is confirmed by our formulations for the density mode of trapped-ion mode scaling case as an example. It is also shown that this mode is completely stabilized when the recycling rate approaches to unity. These results were reexamined by time dependent tokamak transport code and were shown to be physically reasonable.

These results show that our basic formulations are well effective to investigate the effect of the density dynamics on the thermal instability. They also provide useful informations to consider the desirable operating condition.

However, there still remain some quentions to be resolved or extended in future to make clearer the effect of the density dynamics on the thermal instability. Especially, it is of primary importance to investigate what sort of density profile will be realized in the future reactor plasma. Simple application of the INTOR scaling law leads to a

very flat density profile. However, if the round density profile is more likely to be realized in the future reactor plasma, some anomalous inward particle flux must be introduced as in the present-day tokamaks. In this case, the growth time, unstable region and feature of the instability will considerably differ from those of INTOR scaling case. Futhermore, it is also necessary to compare these results with the case, where the round density profile is artificially created by pellet injection or neutral beam injection with the complete exhaust of the diffusing particles. The formulation developed here can be simply extended or applied to these cases. Analyses of these cases and comparisons with the results will be reported elsewhere.

Acknowledgements

The authors would like to express their sincere thanks to Drs. T. Hiraoka, N. Fujisawa and all other members of JT-60 planning office for their valuable discussions and encouragements. They also wish to thank Drs. M. Yoshikawa, M. Tanaka, K. Tomabechi, Y. Iso and S. Mori for their continuous encouragements. This work was carried out when one of the authors (A.H) was staying at the Division of Large Tokamak Development of JAERI.

very flat density profile. However, if the round density profile is more likely to be realized in the future reactor plasma, some anomalous inward particle flux must be introduced as in the present-day tokamaks. In this case, the growth time, unstable region and feature of the instability will considerably differ from those of INTOR scaling case. Futhermore, it is also necessary to compare these results with the case, where the round density profile is artificially created by pellet injection or neutral beam injection with the complete exhaust of the diffusing particles. The formulation developed here can be simply extended or applied to these cases. Analyses of these cases and comparisons with the results will be reported elsewhere.

Acknowledgements

The authors would like to express their sincere thanks to Drs. T. Hiraoka, N. Fujisawa and all other members of JT-60 planning office for their valuable discussions and encouragements. They also wish to thank Drs. M. Yoshikawa, M. Tanaka, K. Tomabechi, Y. Iso and S. Mori for their continuous encouragements. This work was carried out when one of the authors (A.H) was staying at the Division of Large Tokamak Development of JAERI.

References

1) Mills R.G., The problem of Control of Thermonuclear Reactors, in Engineering Problem of Fusion Research (Proc. Symposium Los Alamos, 1969), paper B1, Los Alamos Scientific Laboratory Report LA-4250 (1969).
2) Ohta M., Yamato H., Mori S., in Plasma Physics and Controlled Nuclear Fusion Research (Proc. 4th Int. Conf. Madison, 1971) Vol.3, IAEA, Vienna (1971) 423.
3) Yamato H., Ohta M., Mori S., Nucl. Fusion 12 (1972) 604.
4) Ohta M., Yamato H., Mori S., J. Nucl. Sci. Technol., 10 (1973) 353.
5) Ohnishi M., Yoshikawa H., Wakabayashi J., Nucl. Fusion 13 (1973) 761.
6) Kolesnichenko Ya.I., Reznik S.N., Nucl. Fusion 13 (1973) 167.
7) Stacey W.M., Nucl. Fusion 13 (1973) 843.
8) Fujisawa T., Nucl. Fusion 14 (1974) 173.
9) Stacey W.M., Nucl. Fusion 15 (1975) 63.
10) Kolesnichenko Ya.I., Reznik S.N., in Plasma Physics and Controlled Nuclear Fusion Research (Proc. 6th Int. Conf. Berchtesgaden, 1976) Vol.3, IAEA, Vienna (1977) 347.
11) Kolesnichenko Ya.I., Reznik S.N., Nucl. Fusion 18 (1978) 1535.
12) Bromberg L., Cohn D.R., Fisher J.L., Nucl. Fusion 19 (1979) 1359.
13) Bromberg L., Fisher J.L., Cohn D.R., Nucl. Fusion 20 (1980) 203.
14) Fuchs V., Harten L., Bers A., Nucl. Fusion 20 (1980) 630.
15) Bromberg L., Cohn D.R., Nucl. Fusion 31 (1981) 201.
16) Petrie T.W., Rawls J.M., Nucl. Fusion 20 (1980) 1461.
17) Harten L., Fuchs V., Bers A., Nucl. Fusion 20 (1980) 833.
18) Ashby D.E.T.F., Hughes M.H., Nucl. Fusion 20 (1980) 451.
19) Bromberg L., Cohn D.R., Nucl. Fusion 21 (1981) 110.
20) Borrass K., Minardi E., in European Contributions to the 3rd INTOR Workshop of Phase IIA (1982); Borrass K., Max-Planck-Institute für Plasma Physik, Report IPP 4/189, (1980).
21) INTOR Group, International Tokamak Reactor Zero Phase Report, IAEA, Vienna (1980).
22) Sugihara M., Abe T., Nucl. Fusion 21 (1981) 1024.
23) Seki Y., Shimomura Y., Maki K., Azumi M., Takizuka T., Nucl. Fusion 20 (1980) 1213.

24) Houlberg W.A., Conn R.W., Nucl. Fusion 19 (1979) 81.

25) Ware A.A., Phys. Rev. Lett. 25 (1970) 916.

26) Kobayashi T., Tazima T., Tani K., S. Tamura, JAERI-M 7014 (1977) [in Japanese].

27) Glasstone S., Loverg R.H., Controlled Thermonuclear Reactions, Van Nostrand (1960) 19.

28) Houlberg W.A., Attenberger S.E., Hively L.M., ORNL/TM-7948/V1 (1981).

29) INTOR Group, International Tokamak Reactor Phase 1 Report, IAEA, Vienna (1982).

Table 1 Device parameters of Fusion Experimental Reactor (FER) of JAERI

a (Minor radius)	1.1 m
R (Major radius)	5.5 m
B_t (Toroidal field on axis)	5.7 T
I_p (Plasma current)	5.3 MA
K (ellpticity)	1.5

Table 2 Device and plasma parameters to investigate the density mode of the trapped ion scaling case

a (Minor radius)	1.4 m
R (Major radius)	5.5 m
B_t (Toroidal field on axis)	5.7 T
I_p (Plasma current)	6.7 MA
$\bar{n}_i$ (Average ion density)	$\sim 1.6 \times 10^{20}$ m^{-3}
$\bar{T}_i$ (Average ion temperature)	~ 7 keV

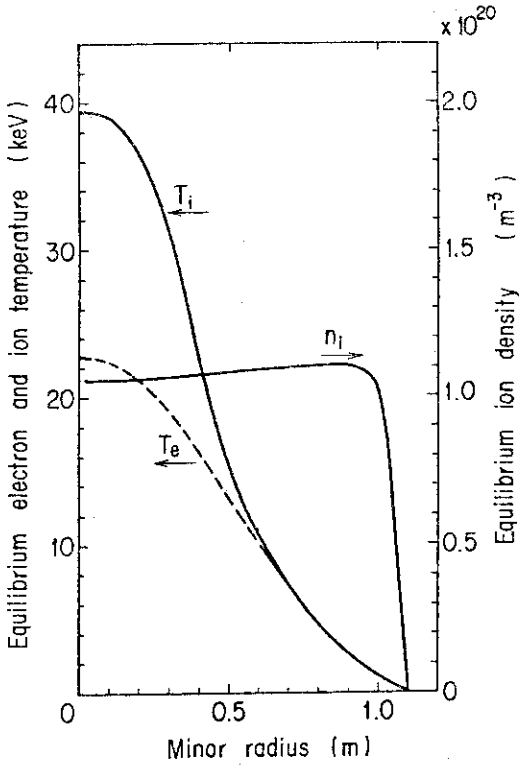

Fig.1 Typical profiles of the electron and ion temperatures and ion density in the steady state of the INTOR scaling case. Average ion and electron temperatures and ion density are $\bar{T}_i \sim 10$ keV, $\bar{T}_e \sim 8$ keV, $\bar{n} \sim 1 \times 10^{20}$ m^{-3}.

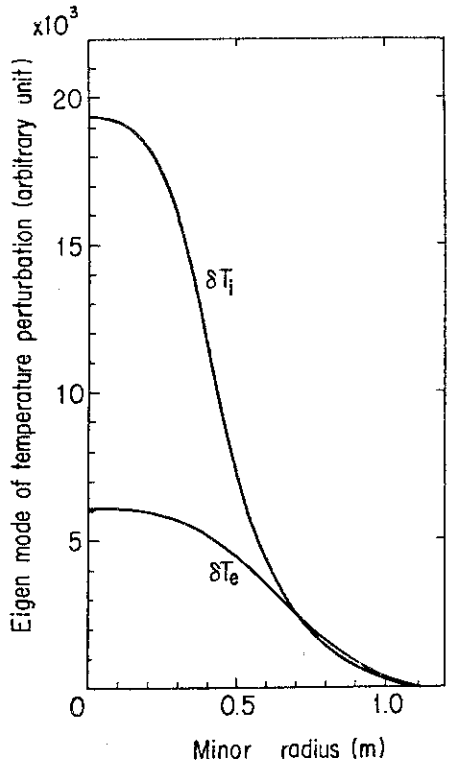

Fig.2 Unstable eigen functions for the ion and electron temperatures in the steady state of Fig.1.

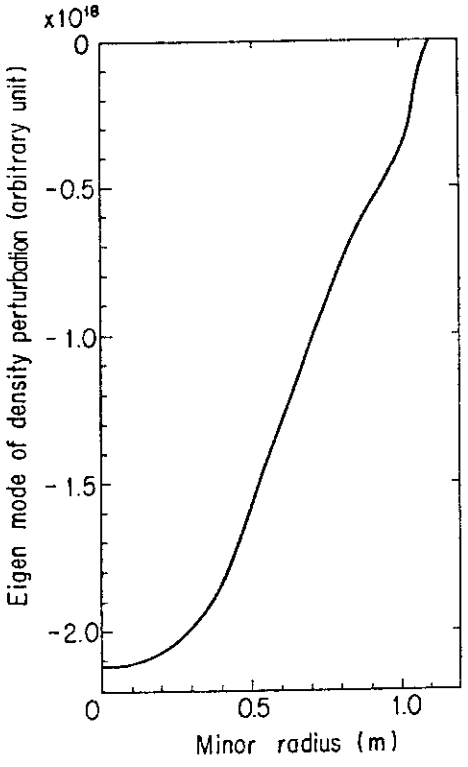

Fig.3 Unstable eigen function for the ion density in the steady state of Fig.1.

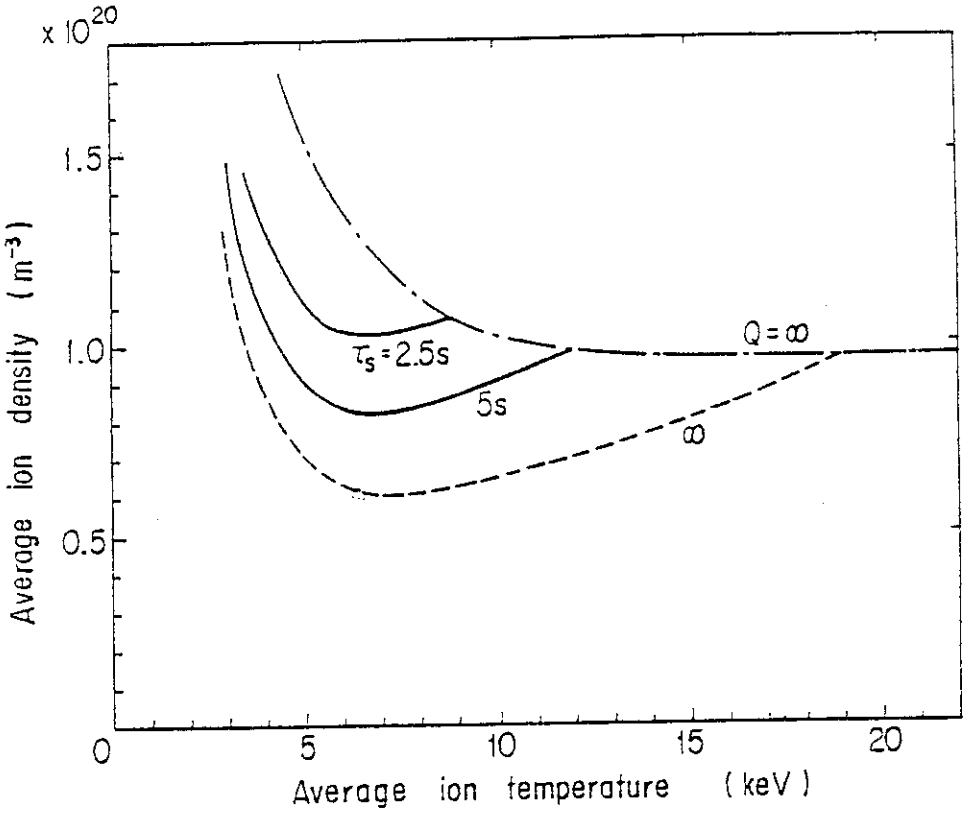

Fig.4 Equi-growth time lines of the instability on $\bar{n}-\bar{T}_i$ plane of the INTOR scaling case. The line of $\tau_s=\infty$ (dotted line) shows the marginal stability. For reference, the ignition line ($Q=\infty$) is also dipicted.

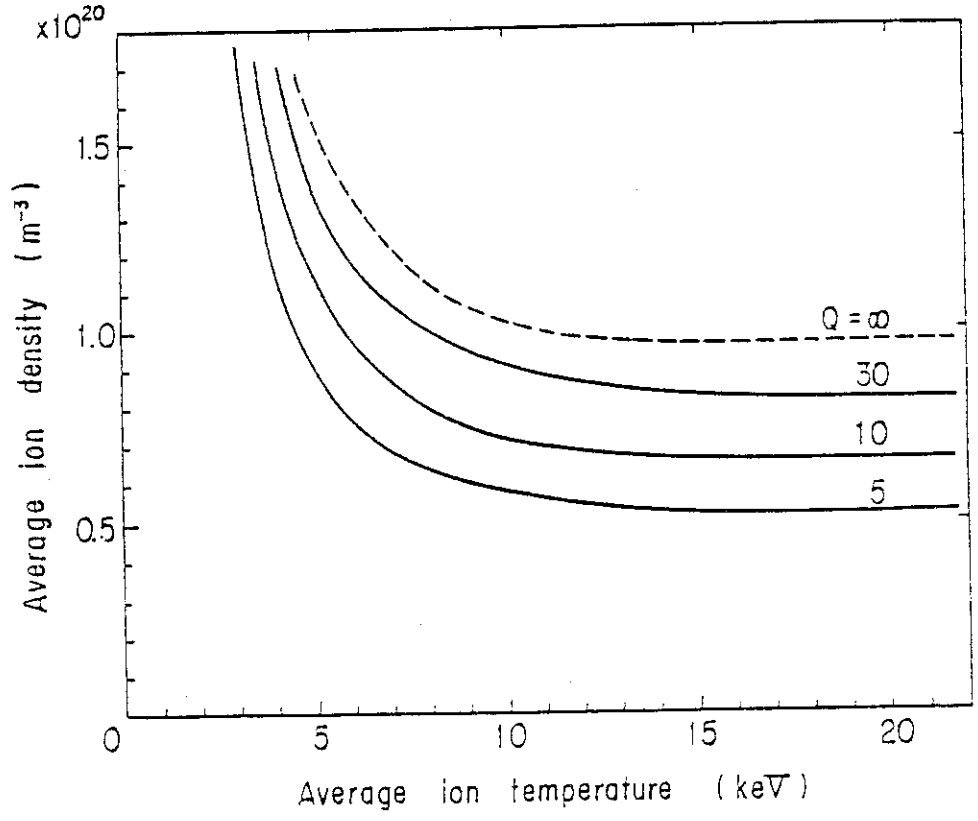

Fig.5 Equi-Q lines of the steady state on $\bar{n}-\bar{T}_i$ plane of the INTOR scaling case. The dotted line shows the self-ignition state.

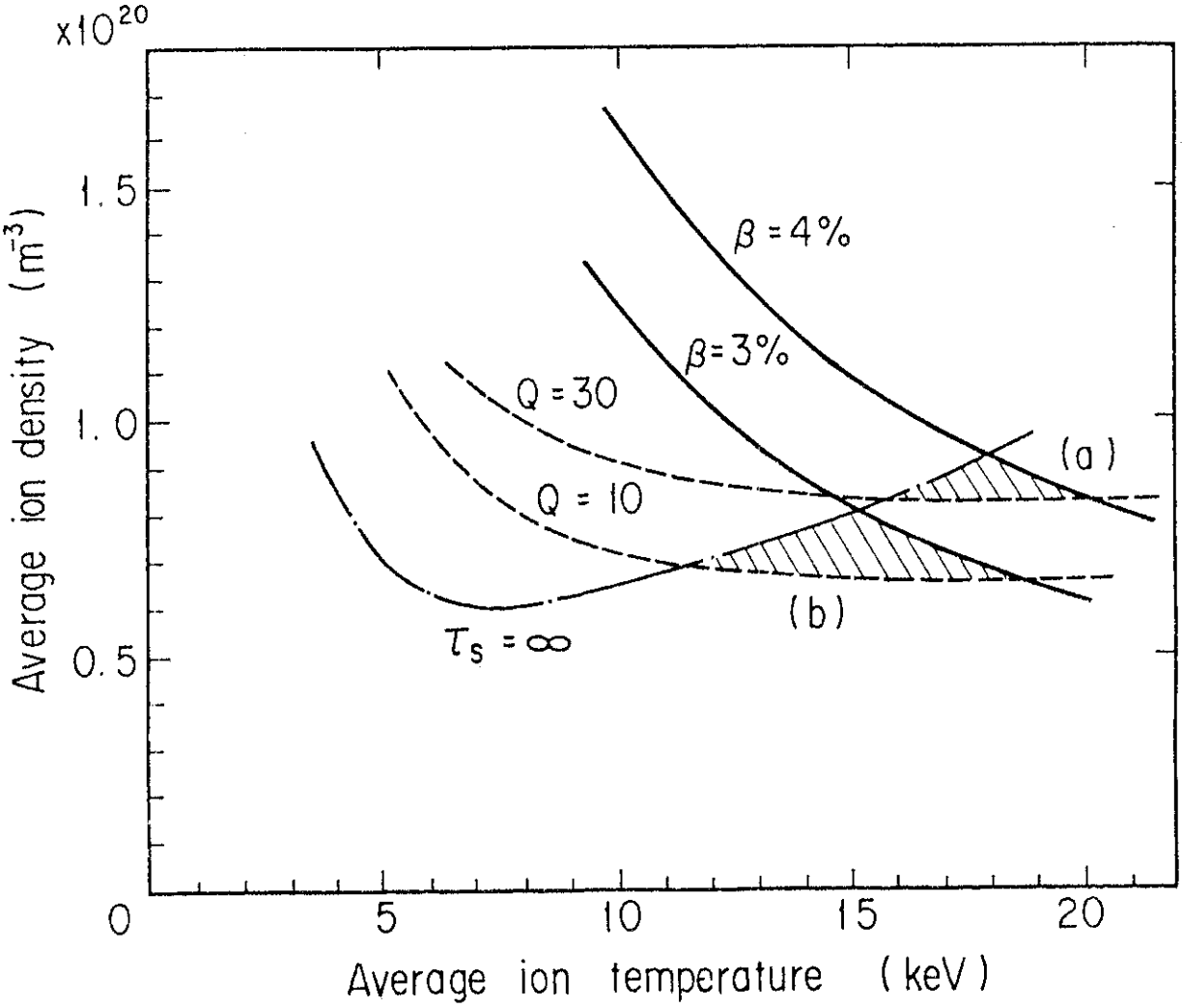

Fig.6 Examples of operating regimes on $\bar{n} - \bar{T}_i$ plane, which satisfy physics design contraints. Constraints imposed are i) thermally stable operation, $Q \geq 30$, $\beta \leq 4\%$ and ii) thermally stable operation, $Q \geq 10$, $\beta \leq 3\%$. They correspond to the hatched regions (a) and (b) in the figure, respectively.

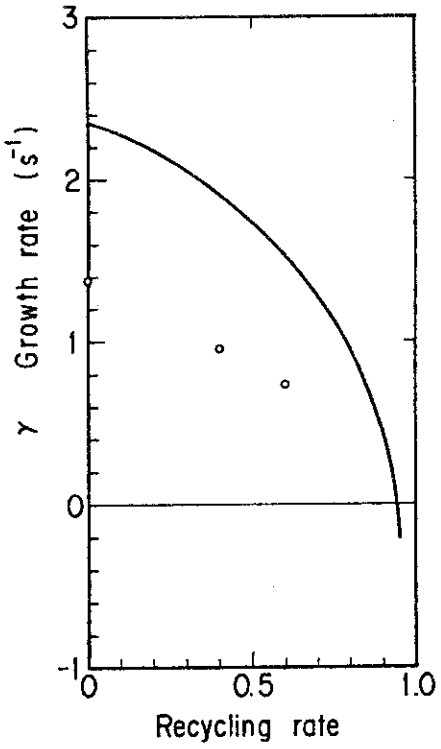

Fig.7 Growth rate of the instability of the trapped ion mode scaling case as a function of the recycling rate. Open circles show the growth rates calculated by the time dependent transport code.

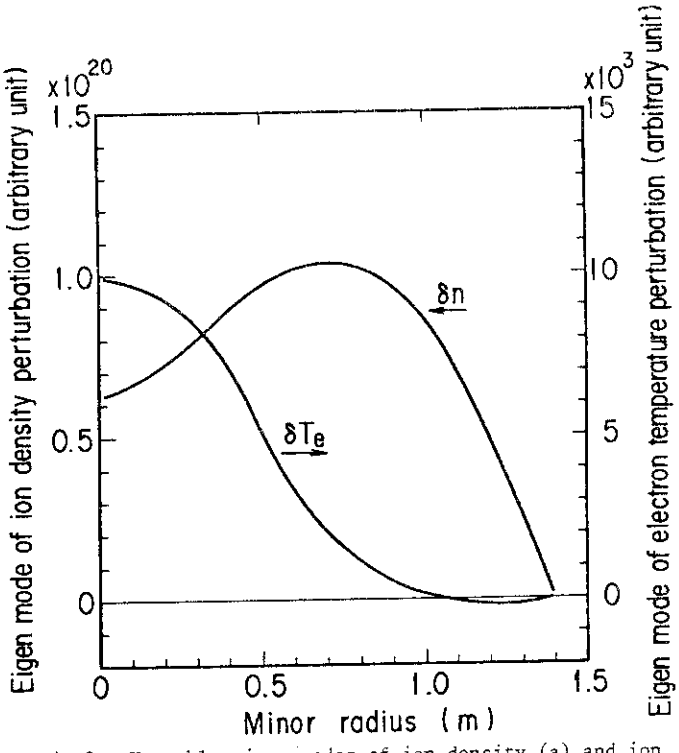

Fig.8 Unstable eigen modes of ion density (a) and ion temperature (b) of the trapped ion mode scaling case for $R_c = 0.0$.

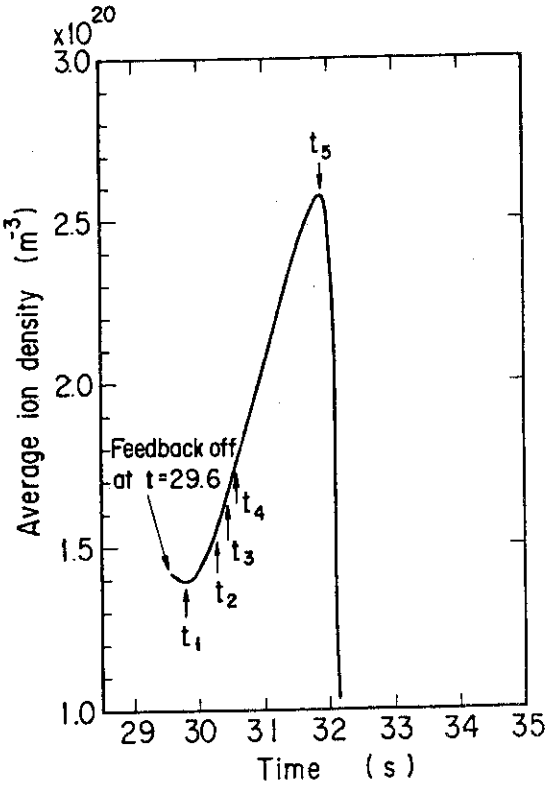

Fig.9 Time evolutions of the average ion density after the eigen mode perturbations shown in Fig.8 are added to the equilibrium state. The feedback control of the density is turned off simultaneously. This result is obtained by the time dependent transport code.

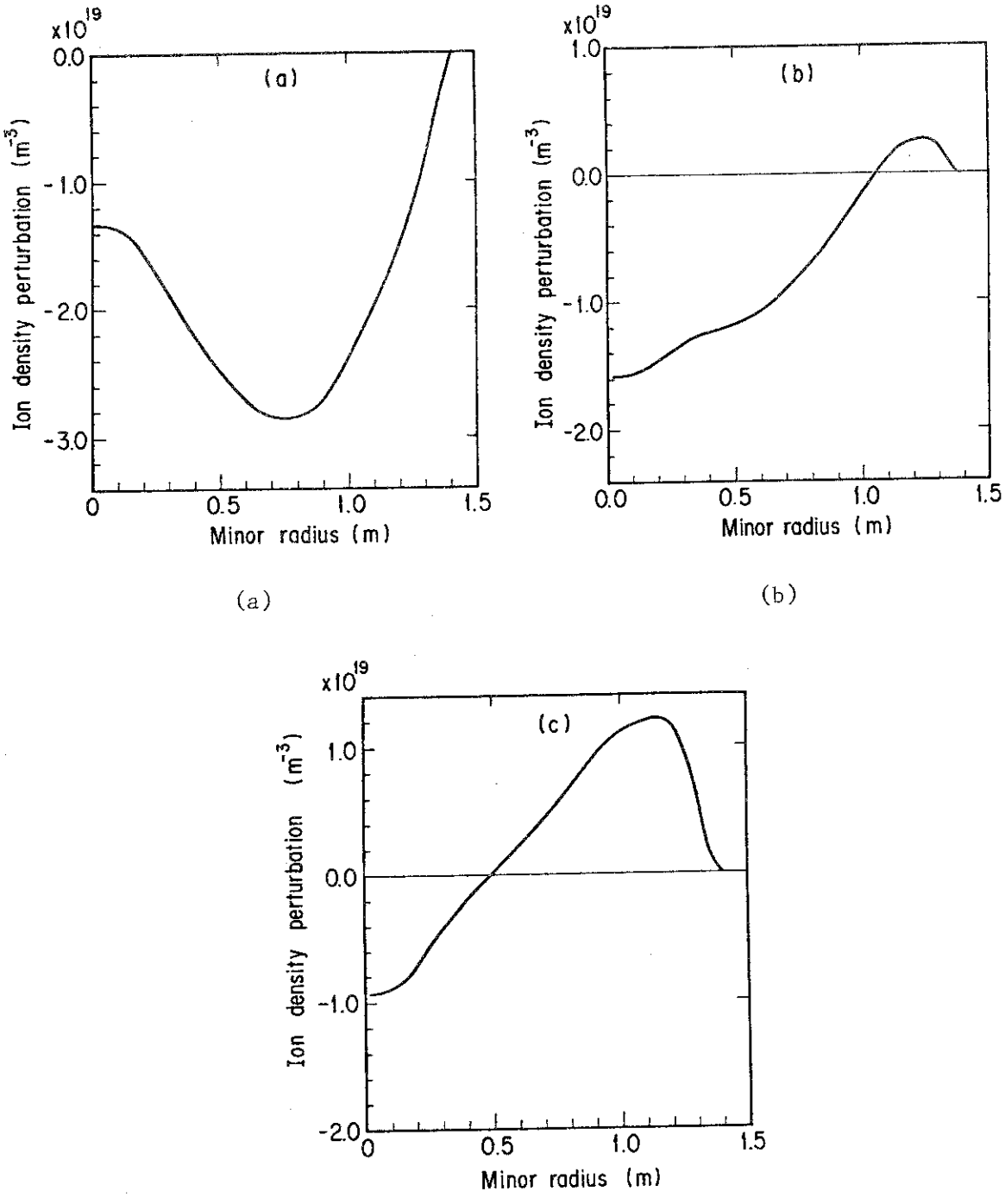

Fig.10 Time evolutions of the density perturbation after the eigen mode perturbation of Fig.8 are added to the equilibrium state. Figures (a) ~ (e) show the perturbations from the equilibrium state at each time $t_1 \sim t_5$ of Fig.9.

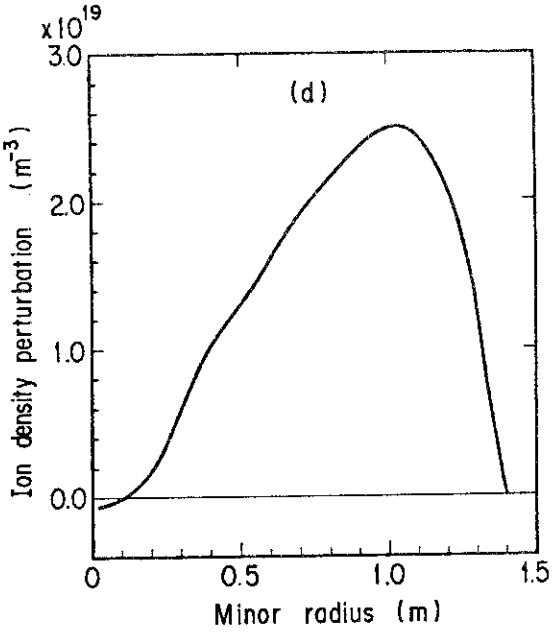

(d)

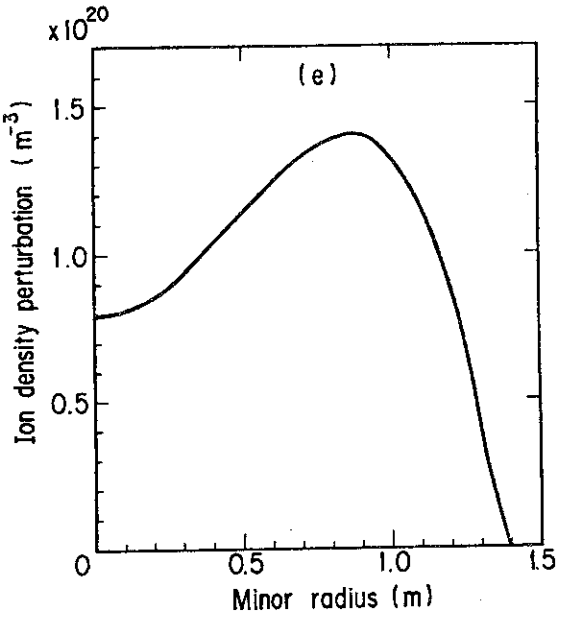

(e)

Fig.10 (Continued)

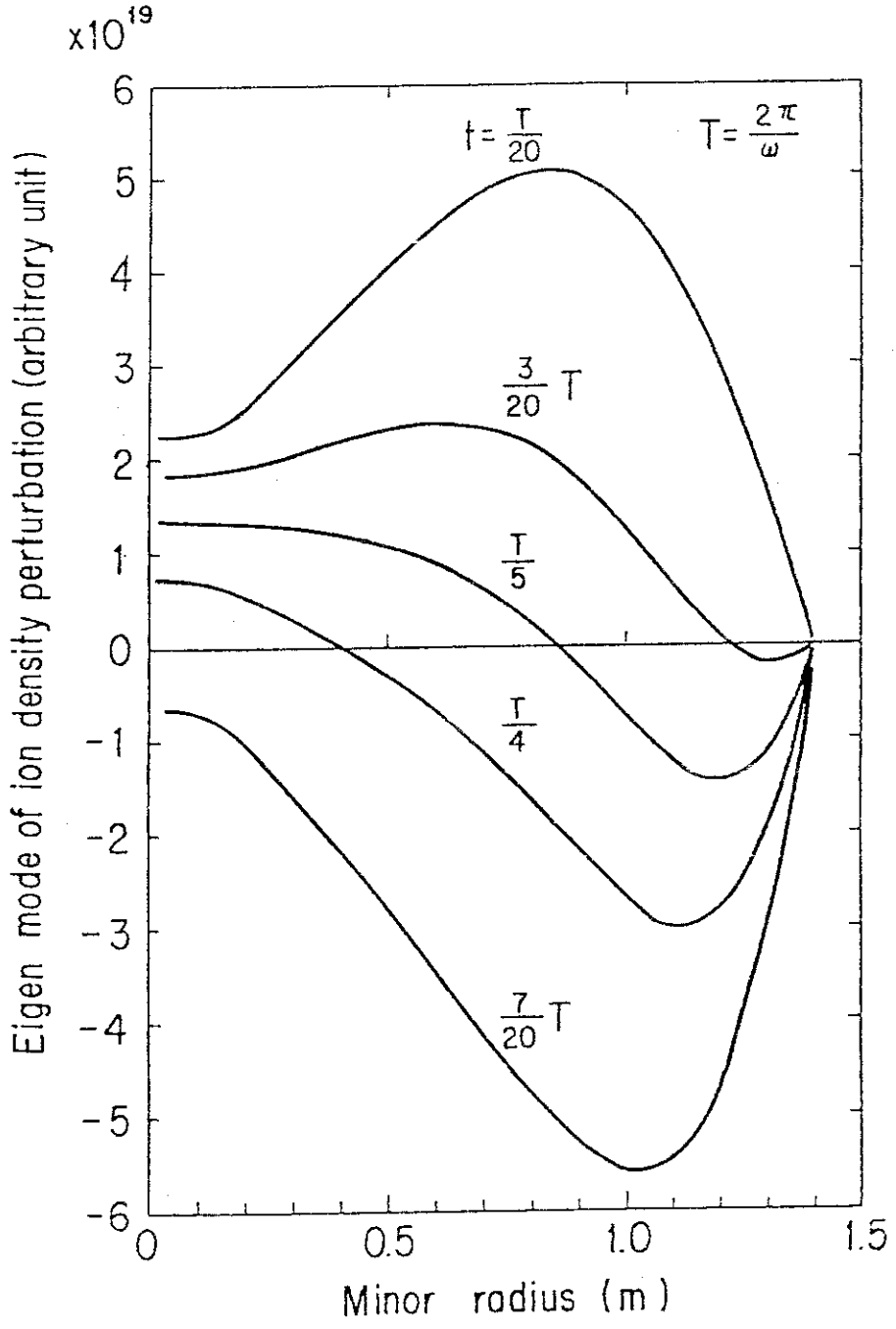

Fig.11 Real part of the unstable eigen functions of Fig.8 for various phases with the growing term (exponential term) dropped. T is the period of the oscillation ($T = 2\pi/\omega \sim 2.4$ s).